Pixel2Mechanics: Automated biomechanical simulations of high-resolution intervertebral discs from anisotropic MRIs

Sai Natarajan[1,2†][0009−0001−4973−2929], Estefano Muñoz-Moya[2†][0000−0001−5222−4071], Carlos Ruiz Wills[2][0000−0002−7475−8557], Gemma Piella[2][0000−0001−5236−5819], Jérôme Noailly[2][0000−0003−3446−7621], Ludovic Humbert[1,3][0000−0002−3675−7908], and Miguel A. González Ballester[2,4][0000−0002−9227−6826]

[1] Galgo Medical S.L., Barcelona, Spain
sai.natarajan@3d-shaper.com
[2] BCN MedTech, Department of Engineering, Universitat Pompeu Fabra, Barcelona, Spain
[3] 3D-Shaper Medical S.L., Barcelona, Spain
[4] ICREA, Barcelona, Spain

Abstract. The intervertebral disc (IVD) degeneration poses demanding challenges for improved diagnosis and treatment personalization. Biomechanical simulations bridge the gap between phenotypes and functional mechanobiology. However, personalized IVD modeling is hindered by complex manual workflows to obtain meshes suitable for biomechanical analysis using clinical MR data. This study proposes Pixel2Mechanics: a novel pipeline for biomechanical finite element (FE) simulation of high-resolution IVD meshes out of low-resolution clinical MRI. We use our geometrical deep learning framework incorporating cross-level feature fusion to generate meshes of the lumbar Annulus Fibrosus (AF) and Nucleus Pulposus (NP) from the L1-L2 to L4-L5 IVD. Further, we improve our framework by proposing a novel optimization method based on differentiable rendering. Next, a custom morphing algorithm based on the Bayesian Coherent Point Drift++ approach generates volumetric FE meshes from the surface meshes, preserving tissue topology through the whole cohort while capturing shape specificities. Daily load simulations on these FE model simulations were evaluated in three volumes within the IVD: the center of the NP and the two transition zones (posterior and anterior) on mechanical responses. These were compared with the results obtained with a manual segmentation procedure. This study delivers a fully automated pipeline performing patient-personalized simulations of L1-L2 to L4-L5 IVD spine levels from clinical MRIs. It facilitates functional modeling and further exploration of normal and pathological discs while minimizing manual intervention. These features position the pipeline as a promising candidate for future clinical integration. Our data & code will be made available at: Pixel2Mechanics

†: These authors contributed equally to this work and are considered co-first authors.

Keywords: Intervertebral Discs · Deep Learning · Differentiable Rendering · Finite Element · Morphing

1 Introduction

Low back pain is a widespread disorder affecting a significant proportion (60-80%) of the global population at some point in their lives [20]. Magnetic Resonance Imaging (MRI) has become the gold standard for diagnosing intervertebral disc (IVD) degeneration (IDD). However, MRI scans are often acquired as multiple thick slices at different orientations, leading to anisotropic voxels that limit accurate 3D anatomical analysis and are unsuitable for biomechanical modeling that relies on high-resolution 3D meshes of the anatomy [4].

In the literature, several studies report biomechanical modeling of the lumbar region from medical imaging modalities. Chen *et al.* [3] developed a deep-learning approach to segment the L4-L5 region of the lumbar spine. Recently, Kok *et al.* [8] proposed a method to model the vertebra and the discs. They first trained a model to generate Synthetic Computed Tomography (SCT) scans from isotropic MRI volumes to segment the vertebra and another model to segment the IVDs from these MRI volumes. However, the above studies involve high-resolution isotropic MRIs that are not clinically easy to obtain and might not be ideal solutions for further translation into accessible modeling tools. Cai *et al.* [1] developed a method to study the biomechanical effects of the L4-L5 IVDs. However, the model was built using a CT scan of a single patient, and the model was modified to construct Finite Element (FE) models based on three variables: disc height, formation of anterior osteophytes, and area of NP. Also, the evaluation was done only for the L4-L5 region and not the entire lumbar spine region. Galbusera *et al.* [6] presented techniques to segment, build FE meshes, and assess the mechanical properties of tissues from imaging data. However, as mentioned above, manual segmentations are time-consuming and delay biomechanical simulations.

FE models and simulations have already led to advanced insights in early IDD, such as possible perturbations of indirect mechanotransduction phenomena when mechanical loads and internal IVD mechanics alter the transport of nutrients to NP cells [15]. However, assessing the variability of internal disc mechanics in a patient-personalized (PP) IVD model way remains a challenge, mainly due to the limitations of simplified geometries [10]. Addressing this, a recent study has delved into morphology's effects on mechanics through FE analysis [5]. Yet, this research solely focused on the outer surface of the AF during the morphing process and overlooks the IVD's internal structure, such as the NP. On the other hand, Muñoz-Moya *et al.* [12] addressed this problem by integrating all the IVD tissues to consider the non-linear interactions between phenotypes and mechanics.

Our study introduces Pixel2Mechanics, a pipeline that combines high-resolution IVD reconstruction from clinical MRI [13], and our morphing algorithm [12] to create customized computer simulations of the IVD, considering both AF and NP. Unlike traditional methods, our pipeline generates these simulations using only anisotropic MRI data as input. It precisely adapts a tissue-structured

generic FE mesh to the unique anatomical details of the patient's IVD, ensuring tailored simulations. To verify the accuracy of these personalized simulations, we compare them with simulations achieved with models from manual segmentations, confirming their accuracy and effectiveness. In this paper, we tackle the above limitations and summarize our contributions below:

- We propose Pixel2Mechanics, a deep learning-based pipeline to reconstruct AF and NP meshes of the L1-L2 to L4-L5 IVDs and perform FE simulations
- We propose a novel differentiable rendering-based optimization to reconstruct AF and NP meshes from clinical MRIs using graph neural networks
- The reconstructed AF and NP meshes are used to generate PP models for FE simulations to evaluate the variability of internal mechanical responses, including inter-personal variability.

2 Methods

The Pixel2Mechanics pipeline, illustrated in Figure 1 (A), begins with the 3D high-resolution mesh reconstruction from anisotropic MRI using [13]. This is followed by morphing via our algorithm and concludes with FE simulations in Abaqus 2020, employing the Sub_disc.f, a User MATerial (UMAT) Fortran subroutine entirely explained in the work [12].

2.1 MRI2Mesh

Image Encoder: To capture PP features from the input MRI volume, we employ a 3D-ResNet50 encoder. It takes a T2-w sagittal sequence as input and extracts patient-level features associated with the discs. The architecture comprises a series of interconnected blocks, each incorporating convolutional, batch normalization, and rectified linear unit (ReLU) layers interspersed with residual connections. The output is a feature vector encoding the PP disc characteristics.

Mesh Deformation: The subsequent component in our architecture comprises graph convolutional neural networks (GCNs). The GCNs receive a template mesh representing an IVD and its associated vertex attributes. The vertex attributes are extracted from the encoder's output using perceptual feature pooling. Our network encompasses three stages of mesh deformation. Each stage undergoes three sequential graph convolutional layers, generating per-vertex offsets relative to the previously deformed mesh reconstruction step.

Cross-level Feature Fusion: Our architecture employs Cross-level Feature Fusion blocks to incorporate local shape features while simultaneously harnessing the global context from optimizing other IVDs. These blocks are strategically positioned after each mesh deformation stage to capture shape-level information effectively. The feature fusion blocks leverage a hybrid approach incorporating convolutional and transformer-based operations. The convolution operations learn the local semantics, while the attention mechanism learns the global context.

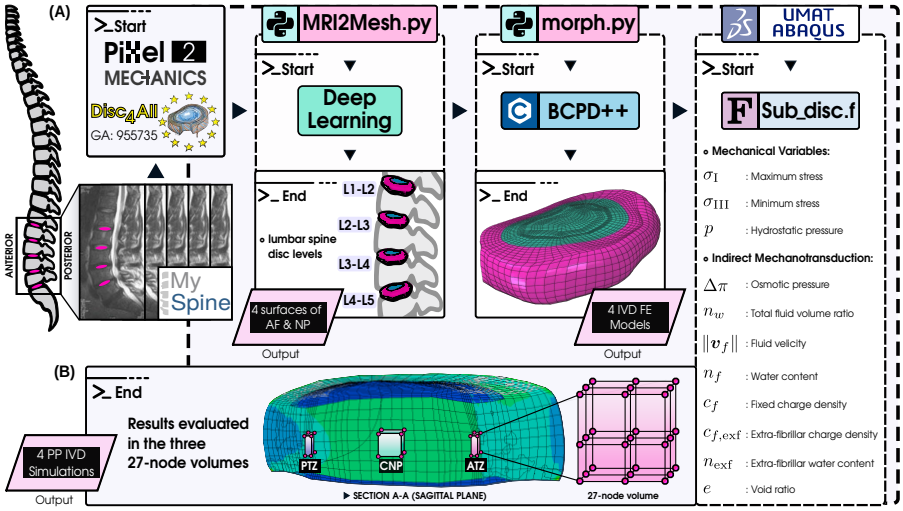

Fig. 1. Pixel2Mechanics framework: The pipeline starts with extracting high-resolution surface meshes of IVDs from anisotropic T2-w sagittal MRI, and later, they are morphed into the generic FE mesh [16] using BCPD++. The process ends by performing the simulation in Abaqus and considering mechanical and indirect mechanotransduction variables. (B) Post-process in which three 27-node volumes are evaluated, PTZ: Posterior transition Zone, CNP: Center of the nucleus pulposus, AT: Anterior transition zone.

2.2 Differentiable Rendering optimization

This section proposes a novel optimization approach for our previous work [13] based on differentiable rendering. A rendering function $\mathcal{R}_f$ takes geometry (shape) parameters θ_s, camera parameters θ_c and lighting parameters θ_l as inputs, and renders images. In our case, these are a silhouette image $\mathcal{I}_s$ and a depth image $\mathcal{I}_d$. We denote the inputs to the renderer as $\theta = \{\theta_s, \theta_c, \theta_l\}$ and the outputs as $\mathcal{I} = \{\mathcal{I}_s, \mathcal{I}_d\}$. Figure 2 displays the optimization process using differentiable rendering. The renderer takes as input θ and produces outputs $\mathcal{I}$ corresponding to scene parameters and the type of renderer. The camera and light settings are fixed across the shapes during training and are not optimized. The images are rendered at a resolution of 256×256. For each shape, views are captured from different angles during each iteration, and the loss is computed with the ground truth silhouette and depth images.

2.3 Objective function

Finding an estimate of shape and appearance is formulated as a minimization problem. Our total loss is composed of an appearance loss and geometric loss. The appearance loss is composed of two terms $\mathcal{L}_{silhouette}$ and $\mathcal{L}_{depth}$. $\mathcal{L}_{silhouette}$ is a Dice loss and is calculated between the rendered silhouette and the ground truth silhouette images. $\mathcal{L}_{depth}$ is computed by measuring the $L1$ distance between

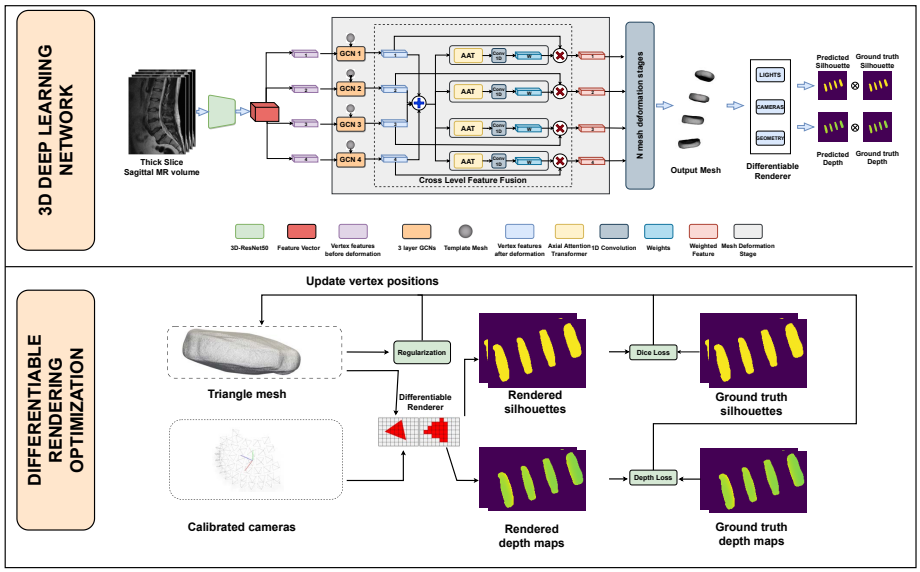

Fig. 2. The architecture of our 3D reconstruction network (top) and the optimization procedure using differentiable rendering (bottom)

the rendered depth map and the ground truth depth map to enhance geometric consistency. Both are averaged over a set of calibrated renderings. Deforming vertices unregulated leads to meshes with self-intersections and degenerate triangles, which are undesirable. Therefore, we use two regularization terms. To reconstruct smooth meshes, we use a Laplacian loss that regularizes the difference between a vertex $\mathbf{p}$ of the predicted mesh $\mathbf{P}$ and the mean location of its neighboring vertices $\mathbf{k}_p$ in the neighborhood $\mathcal{N}_p$ and a normal consistency loss given by:

$$\mathcal{L}_{Laplacian}(\mathbf{P}) = \sum_{\mathbf{p}\in\mathbf{P}} \|\mathbf{p} - \sum_{\mathbf{k}_p\in\mathcal{N}_p} \frac{1}{|\mathcal{N}_p|}\mathbf{k}_p\|_2^2 \tag{1}$$

$$\mathcal{L}_{normal} = \frac{1}{|\hat{\mathcal{F}}|} \sum_{i,j\in\hat{\mathcal{F}}} (1 - \mathbf{n}_i \cdot \mathbf{n}_j)^2 \tag{2}$$

where $\hat{\mathcal{F}}$ is the set of pairs of triangles that have a common edge and $\mathbf{n_i} \in \mathbb{R}^3$ is the normal of triangle i.

2.4 Biomechanical Simulation

The disc morphologies derived from our deep learning network are further used in FE simulations, emulating the average daily compressive loading of the discs, derived from *in vivo* intradiscal pressure measurements in [19]. These compressive loads are 0.11 MPa for the night and 0.54 MPa for the day during two days, as

was specified in the methodology in [12]. We compared the simulation outcomes from our pipeline versus those derived from manual segmentation to ascertain the efficacy of Pixel2Mechanics. A set of five personalized IVD model geometries with heights ranging from $\sim$ 8-16 mm resulted from a morphing process that adjusted a standardized FE IVD mesh to the specific morphological characteristics of each disc. The structure of the mesh was tissue-specific and verified against mesh convergence analysis in [15], with subsequent validations performed in [9] and [12], building upon an original structured model in [14]. [12] provides an in-depth description of this process, which employs Bayesian Coherent Point Drift++ [7]. The Hausdorff distance evaluates the similarity score between the generated models and the morphed ones, as [12] indicates. The biomechanical properties assigned to the models are characterized by an osmo-poro-hyper-viscoelastic material model, outlined in [12].

3 Experiments

Dataset: We used 150 T2-w sagittal volumes from the former project MySpine (FP7-ICT-2009-6-269909) obtained from CETIR, Barcelona, Spain, and NCSD, Budapest, Hungary. The sagittal and coronal volumes were fused as done in [2] to obtain a high-resolution volume and were annotated by clinical experts. This was done solely to obtain the ground truth meshes, which were not used for training and testing. All the scans have a resolution of 0.68×0.68 mm and a slice thickness of 4.0 mm or 4.4 mm. We use Adam as the optimizer with a learning rate of $2e^{-4}$ with a PolyLR learning rate decay. We performed a 3-fold cross-validation training strategy with 100 volumes for training, 20 for validation, and 30 for testing. A subset of this test set consisting of L1-L2 to L4-L5 IVDs (four discs) of a single patient was used to test the FE mesh generation tool. Five L4-L5 IVDs from different patients were used to perform the biomechanical simulations.

Models obtained via manual segmentation, previously simulated with the same characteristics of this study in [12], are accessible through the SpineView[‡] online user interface [11]. The results of the simulations were evaluated in three 27-node volumes (Figure 1B) for early IDD states [12], such as the posterior transition zone (PTZ), the center of the nucleus pulposus (CNP), and the anterior transition zone (ATZ), selected because they might stand for local sites of early damage [17]. A comparative analysis of these results was then conducted between the models from our deep learning network and the counterpart models from manual segmentations.

To evaluate the feasibility of our tool, we implemented a comparative analysis of the calculated mechanical responses—maximum and minimum stresses and hydrostatic pressure (σ_{I}, σ_{III}, p)—against the posterior, middle, and anterior heights (PH, MH, and AH). This method was inspired by the findings in [12], who identified a significant correlation between mechanical behaviors and morphological characteristics. The research highlighted that although specific local

[‡] https://ivd.spineview.upf.edu/

morphologies may dominate within distinct sectors, the mechanical diversity is significantly shaped by the morphology of neighboring areas.

4 Results

4.1 IVD reconstruction

To our knowledge, no prior deep-learning networks can reconstruct anatomical shapes using differentiable rendering. We compare our results to Voxel2Mesh [18] for direct mesh reconstruction from volume. It was adapted to train on a differentiable rendering setting, i.e., we removed the 3D decoder network that outputs the 3D segmentation as it is unfair to simultaneously train the model with 3D segmentation and 2D renderings. Segmentation approaches were studied in [13] and the findings indicate that although Dice scores benefit the segmentation models, they are constrained by slice thickness and voxel coordinate system. This makes it challenging to accurately model the degenerated discs in L34 and L45 regions as illustrated in Figure S2 of the supplementary material. We compare our results with the ground truth meshes through Hausdorff Distance (HD) and Point-to-Surface (P2S).

Quantitative results for IVD components AF and NP meshes are presented in Table 1. Our method with differentiable rendering scored an average Hausdorff distance of 4.03 ± 0.74 mm and an average Point-to-Surface (P2S) distance of 2.26 ± 0.65 mm performing better than Voxel2Mesh, which scored 4.76 ± 1.03 mm for Hausdorff distance and 2.81 ± 0.96 mm for the Point-to-Surface distance. Compared to AF reconstruction, generating NP meshes is challenging. Accurately detecting NP within the intervertebral disc (IVD) using a low-resolution MRI image presents a significant challenge. This is evident in the reconstruction results in Table 1. Figure S1 in supplementary material shows further examples of qualitative comparison of our cross-level feature fusion with Voxel2Mesh.

Table 1. Reconstruction results for the AF and NP meshes with their std. error in mm

Method	HD (AF)	P2S (AF)	HD (NP)	P2S (NP)
Voxel2Mesh (DR)	4.76 ± 1.03	2.81 ± 0.96	5.01 ± 1.13	$\mathbf{2.80 \pm 1.12}$
Ours	$\mathbf{4.03 \pm 0.74}$	$\mathbf{2.26 \pm 0.65}$	$\mathbf{4.93 \pm 0.94}$	2.81 ± 0.43

4.2 Biomechanical Simulation

The similarity score of the AF and NP for the L4-L5 levels of the patient NC0031 is shown in Table 2. A visual comparison between the reconstructed and morphed models can be found in the supplementary material Figure S3.

The morphological features, simulation results, and similarity scores between the real and morphed models of the L4-L5 spine IVD models generated by the morphing process used in the simulations are delineated in Table 3. A visual comparison can be found in the supplementary material Figure S4.

Table 2. Similarity % for the L1-L2 to L4-L5 levels of the lumbar IVD spine

Similarity %	Tissue	L1L2	L2L3	L3L4	L4L5
	AF	90.71	94.30	93.85	90.88
	NP	88.00	90.71	93.30	88.62

Table 3. The similarity score (S%), heights, and simulation results (maximum σ_{I} and minimum stress σ_{III}, and hydrostatic pressure p) evaluated in the three volumes, CNP, PTZ, and ATZ, of the morphed models with three different heights from highest to lowest. MH: Middle height, PH: Posterior Height, AH: Anterior Height, PTZ: Posterior Transition Zone, CNP: Center of the Nucleus Pulposus ATZ: Anterior Transition Zone.

Model	S %		Disc height (mm)			PTZ (MPa)			CPN (MPa)			ATZ (MPa)		
ID	AF	NP	PH	MH	AH	σ_{I}	σ_{III}	p	σ_{I}	σ_{III}	p	σ_{I}	σ_{III}	p
NC0031	90.88	88.62	6.05	15.99	11.51	-0.205	-0.584	0.221	-0.264	-0.490	0.267	-0.099	-0.529	0.181
NC0092	90.84	91.12	7.94	11.16	8.37	-0.181	-0.571	0.224	-0.298	-0.548	0.276	-0.232	-0.559	0.254
NC0003	93.46	92.77	7.22	9.52	11.15	-0.133	-0.533	0.130	-0.294	-0.564	0.291	-0.127	-0.542	0.222
NC0228	94.37	93.48	5.65	9.42	8.03	-0.146	-0.539	0.185	-0.253	-0.499	0.260	-0.086	-0.432	0.121
NC0225	93.63	93.88	4.06	8.27	6.35	-0.197	-0.520	0.228	-0.282	-0.520	0.274	-0.178	-0.573	0.222

5 Discussion and Conclusion

We present a highly scalable, fully automatic pipeline to generate high-resolution reconstructions of the IVDs from clinical MRI and perform patient-personalized biomechanical simulations. While triangle meshes effectively represent anatomy, they pose challenges in differentiable rendering. We addressed this with geometry regularizers, but balancing smoothness and rendering remains an open question. By simulating the mechanical behavior of the disc under different loads and conditions, these simulations can help identify subtle changes in disc integrity that might not be readily apparent from MRIs alone. We demonstrate that the results generated by this pipeline are highly correlated and agree with those generated by manual segmentations without human-in-the-loop correction.

The study revealed that the four IVDs generated from patient NC0031, along with five discs of varying heights, demonstrated a high similarity score, exceeding 90% for both the AF and NP in nearly all models. These results validate observations in [12], noting the complex relationship between mechanical responses and morphology, indicating that additional morphological aspects influence mechanical responses. This observation extends to the posterior and anterior regions, emphasizing the importance of detailed morphological assessment of the IVD for accurate simulation representation. Consequently, this study underscores the importance of customizing not only the disc height but also the overall morphology to achieve feasible simulations.

This work indicates that automatic reconstructions may effectively substitute human interventions, which are time-intensive and costly to obtain, in offering a reliable alternative for quantifying disc morphology and biomechanical responses.

Acknowledgments. The European Commission funded this research study through the (H2020-MSCA-ITN-ETN-2020) Disc4All (Grant agreement 955735). We also thank the MySpine (FP7-ICT-2009-6-269909) project members for making the data available, the ICREA Academia program, and the ERC CoG O-Health (Grant Agreement: 101044828).

Disclosure of Interests. The authors have no competing interests to declare that are relevant to the content of this article.

Bibliography

[1] Cai, X.y., Sun, M.s., Huang, Y.p., Liu, Z.x., Liu, C.j., Du, C.f., Yang, Q.: Biomechanical effect of l4–l5 intervertebral disc degeneration on the lower lumbar spine: a finite element study. Orthopaedic surgery **12**(3), 917–930 (2020)

[2] Castro-Mateos, I., Pozo, J.M., Eltes, P.E., Rio, L.D., Lazary, A., Frangi, A.F.: 3d segmentation of annulus fibrosus and nucleus pulposus from t2-weighted magnetic resonance images. Physics in Medicine and Biology **59**(24), 7847–7864 (nov 2014)

[3] Chen, T., Su, Z.h., Liu, Z., Wang, M., Cui, Z.f., Zhao, L., Yang, L.j., Zhang, W.c., Liu, X., Liu, J., et al.: Automated magnetic resonance image segmentation of spinal structures at the l4-5 level with deep learning: 3d reconstruction of lumbar intervertebral foramen. Orthopaedic Surgery **14**(9), 2256–2264 (2022)

[4] El Bojairami, I., El-Monajjed, K., Driscoll, M.: Development and validation of a timely and representative finite element human spine model for biomechanical simulations. Scientific Reports **10**(1), 21519 (2020)

[5] Fleps, I., Newman, H.R., Elliott, D.M., Morgan, E.F.: Geometric determinants of the mechanical behavior of image-based finite element models of the intervertebral disc. Journal of Orthopaedic Research (Jan 2024). https://doi.org/10.1002/jor.25788

[6] Galbusera, F., Cina, A., Panico, M., Albano, D., Messina, C.: Image-based biomechanical models of the musculoskeletal system. European radiology experimental **4**(1), 1–13 (2020)

[7] Hirose, O.: Acceleration of non-rigid point set registration with downsampling and gaussian process regression. IEEE Transactions on Pattern Analysis and Machine Intelligence **43**(8), 2858–2865 (Aug 2021). https://doi.org/10.1109/TPAMI.2020.3043769

[8] Kok, J., Shcherbakova, Y.M., Schlösser, T.P., Seevinck, P.R., van der Velden, T.A., Castelein, R.M., Ito, K., van Rietbergen, B.: Automatic generation of subject-specific finite element models of the spine from magnetic resonance images. Frontiers in Bioengineering and Biotechnology **11** (2023)

[9] Malandrino, A., Pozo, J.M., Castro-Mateos, I., Frangi, A.F., van Rijsbergen, M.M., Ito, K., Wilke, H.J., Dao, T.T., Ho Ba Tho, M.C., Noailly, J.: On the relative relevance of subject-specific geometries and degeneration-specific mechanical properties for the study of cell death in human intervertebral disk models. Frontiers in Bioengineering and Biotechnology **3** (2015)

[10] Meijer, G.J.M., Homminga, J., Veldhuizen, A.G., Verkerke, G.J.: Influence of interpersonal geometrical variation on spinal motion segment stiffness: Implications for patient-specific modeling. Spine **36**(14), E929–E935 (Jun 2011). https://doi.org/10.1097/brs.0b013e3181fd7f7f

[11] Muñoz-Moya, E., Rasouligandomani, M., Ruiz Wills, C., Chemorion, F., Piella, G., Noailly, J.: Repository of ivd patient-specific fe models (Sep 2023).

https://doi.org/10.5281/zenodo.8325042, https://doi.org/10.5281/zenodo.8325042

[12] Muñoz-Moya, E., Rasouligandomani, M., Ruiz Wills, C., Chemorion, F.K., Piella, G., Noailly, J.: Unveiling interactions between intervertebral disc morphologies and mechanical behavior through personalized finite element modeling. Frontiers in Bioengineering and Biotechnology **12** (2024). https://doi.org/10.3389/fbioe.2024.1384599, https://www.frontiersin.org/journals/bioengineering-and-biotechnology/articles/10.3389/fbioe.2024.1384599

[13] Natarajan, S., Tiulpin, A., Humbert, L., Ballester, M.A.G.: Mri2mesh: Intervertebral disc mesh generation from low resolution mri using graph neural networks with cross level feature fusion. In: 2023 IEEE 20th International Symposium on Biomedical Imaging (ISBI). pp. 1–5 (2023). https://doi.org/10.1109/ISBI53787.2023.10230651

[14] Noailly, J., Planell, J.A., Lacroix, D.: On the collagen criss-cross angles in the annuli fibrosi of lumbar spine finite element models. Biomechanics and Modeling in Mechanobiology **10**(2), 203–219 (Jun 2010)

[15] Ruiz, C., Foata, B., González Ballester, M.A., Karppinen, J., Noailly, J.: Theoretical explorations generate new hypotheses about the role of the cartilage endplate in early intervertebral disk degeneration. Frontiers in Physiology **9** (2018)

[16] Ruiz, C., Noailly, J., Lacroix, D.: Material property discontinuities in intervertebral disc porohyperelastic finite element models generate numerical instabilities due to volumetric strain variations. Journal of the Mechanical Behavior of Biomedical Materials **26**, 1–10 (Oct 2013). https://doi.org/10.1016/j.jmbbm.2013.05.012

[17] Smith, L.J., Nerurkar, N.L., Choi, K.S., Harfe, B.D., Elliott, D.M.: Degeneration and regeneration of the intervertebral disc: lessons from development. Disease Models & Mechanisms **4**(1), 31–41 (01 2011)

[18] Wickramasinghe, U., Remelli, E., Knott, G., Fua, P.: Voxel2mesh: 3d mesh model generation from volumetric data. In: Medical Image Computing and Computer Assisted Intervention–MICCAI 2020: 23rd International Conference, Lima, Peru, October 4–8, 2020, Proceedings, Part IV 23. pp. 299–308. Springer (2020)

[19] Wilke, H., Neef, P., Caimi, M., Hoogland, T., Claes, L.E.: New in vivo measurements of pressures in the intervertebral disc in daily life. Spine **24**(8), 755–762 (Apr 1999)

[20] Wu, A., March, L., Zheng, X., Huang, J., Wang, X., Zhao, J., Blyth, F.M., Smith, E., Buchbinder, R., Hoy, D.: Global low back pain prevalence and years lived with disability from 1990 to 2017: estimates from the global burden of disease study 2017. Annals of translational medicine **8**(6) (2020)